A. Instruments

A PerkinElmer RXI spectrophotometer was used for recording the FT-IR spectra. Sample concentrations in the KBr pellets was 2 w/w%. NMR spectra were obtained on the Bruker Avance 300 MHz and 400 MHz spectrometers using tetramethylsilane (TMS). Atomic absorption measurements were carried out on a Young Ling AAS 8020. TGA curves were recorded on a Linseis STA PT 1000 for the powdered samples (scanning rate 10°C/min). SEM images were obtained on a MIRA3 FEG-SEM instrument with an acceleration voltage of 30 kV. The TEM images of samples were obtained by using a transmission electron microscope (EM10C, Zeiss) with an acceleration voltage of 80 kV. A Dr. Heilscher high intensity ultrasound processor UP200H Germany (13 mm diameter titanium horn, 200 W/cm^2, 23 kHz) was used for the preparation of magnetite nanoparticles. A Vibrating sample magnetometer with a maximum magnetic field of 10 kOe (VSM, MaghnatisDaghighKavir Co.) was used for magnetization measurements at room temperature. Wide angle X-ray diffraction (XRD) and low angle X-ray diffractograms in 2θ range of 10-80° and 0.7–10° were obtained on Philips PW1730 (scanning rate 0.01°/min) and Philips X-Pro (scanning rate 1°/min) instruments at room temperature, respectively. Both instruments were equipped with an X-ray radiation source using Cu Kα (λ= 0.15406 nm). The specific surface area and pore volume were determined by N_2 adsorption/desorption using a Sorptometer 1900 apparatus (Carlo-Erba Instruments). X-ray photoelectron spectroscopy (XPS) were recorded on a SPECS Phoibos HAS 3500 150 MCD X-ray photoelectron spectrometer. The X-ray source was a monochromatic Al anode (1486.7 eV). The pass energy was set to 120 and 50 eV for the survey and the narrow regions, respectively. Accurate binding energies have been determined with respect to the position of C1s at 285 eV. Quantitative GC analyses were performed with an Agilent 7890 instrument using a capillary column in conjunction with a flame ionization detector (GC/FID). The column temperature was programmed between 180and 200°C

(2°C/min). Activity of Fe_3O_4@SiO_2@SBA-PyBzIm-Pd(0)was represented in terms of reaction yields. Nitrogen was used as a carrier gas at a flow rate of 20 mL/min.

B. Materials

Nanoparticles of Fe_3O_4 [1], Fe_3O_4@SiO_2-SBA-15 nanocomposite [2, 3], and trans-[$Pd(Cl)_2(SMe_2)_2$] complex [4] were prepared according to the literature reported methods. 3-Aminopropyltrimethoxysilane (APTES) was obtained from Exir (Austria). Pluronic P123, tetraethyl orthosilicate (TEOS), 3-aminoopropyltriethoxysilane (APTES), and $PdCl_2$ were obtained from Sigma-Aldrich and used without further purification. Laboratory grade solvents used in this work were dried according to the literature reported procedures [5]. The remaining chemicals were obtained from Merck.

C. Synthesis of Fe_3O_4@SiO_2-SBA-15

Magnetite nanoparticles were synthesized via the co-precipitation method under ultrasonic irradiation. The as-prepared magnetite nanoparticles were then encapsulated in a silica shell, and then impregnated into channels of SBA-15 [2, 6]. Figure S1 displays the low-angle XRD pattern of the Fe_3O_4@SiO_2@SBA-15. The distinct characteristic diffraction peak at $2\theta = 1.06°$ corresponds to (100), and confirms the formation of mesoporous ordered hexagonal structure of SBA-15 with the P6mm space group [7]. The weak diffraction peaks corresponding to (110) and (200) are absent probably due to disordering SBA channels by magnetite nanoparticles [8, 9]

Figure S1. Low angle powder XRD pattern of Fe_3O_4@SiO_2@SBA-15.

MNPs were prepared via the co-precipitation method under ultrasonic irradiation. In the transmission electron microscopy (TEM) image of the prepared magnetite, the uniform spherical shapes nanoparticles with the diameter, Figure S2-a. The average particle size of Fe_3O_4 was found to be about 9 nm. The ImageJ analysis software derives the estimation by random selecting of 10 nanoparticles in the TEM image. The as-prepared magnetite nanoparticles were then encapsulated in a silica shell and impregnated into SBA-15 channels [2]. TEM image shows the ordered structure of magnetic SBA. A dispersion of Fe_3O_4 nanoparticles (of diameter 20-50 nm) between highly ordered channels of SBA-15 is seen in Figure S2-b.

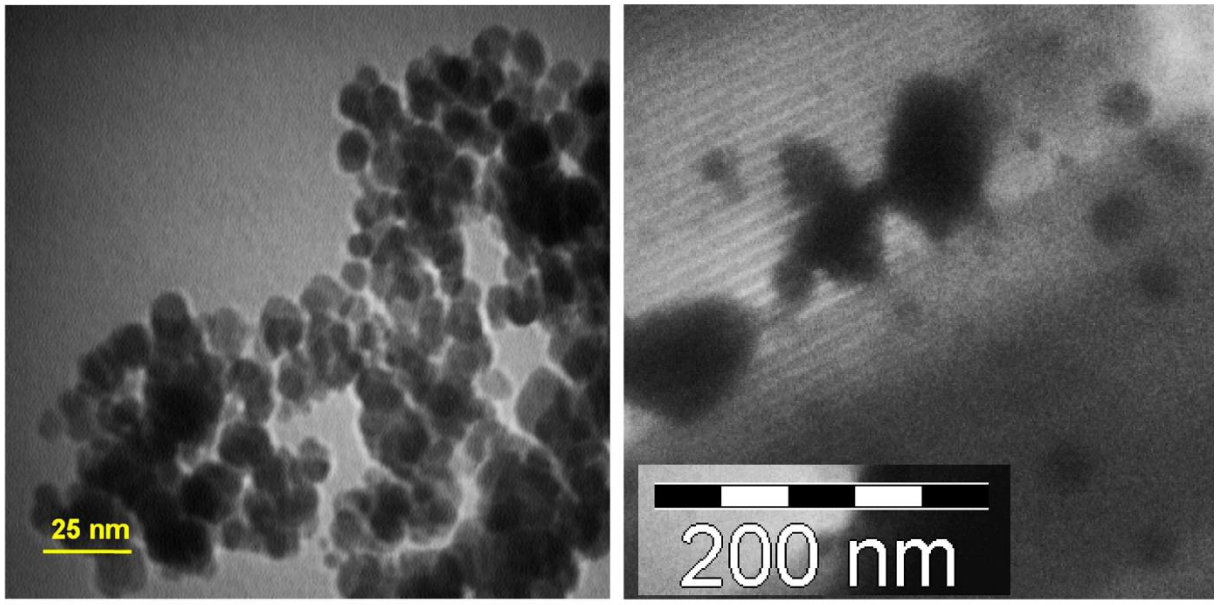

(a) **(b)**

Figure S2. TEM images of: (a) Fe_3O_4 nanoparticles; and Fe_3O_4@SBA.

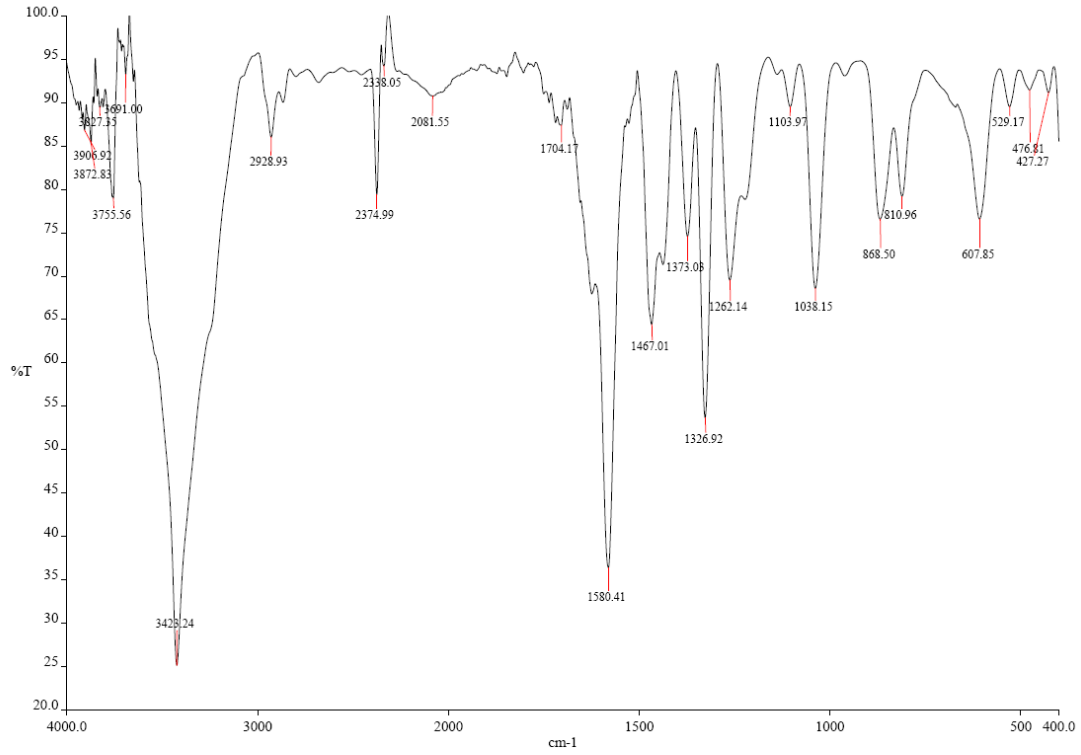

Figure S3. FT-IR spectrum of 4-hydroxyacetophenone oxime-derived palladacycle.

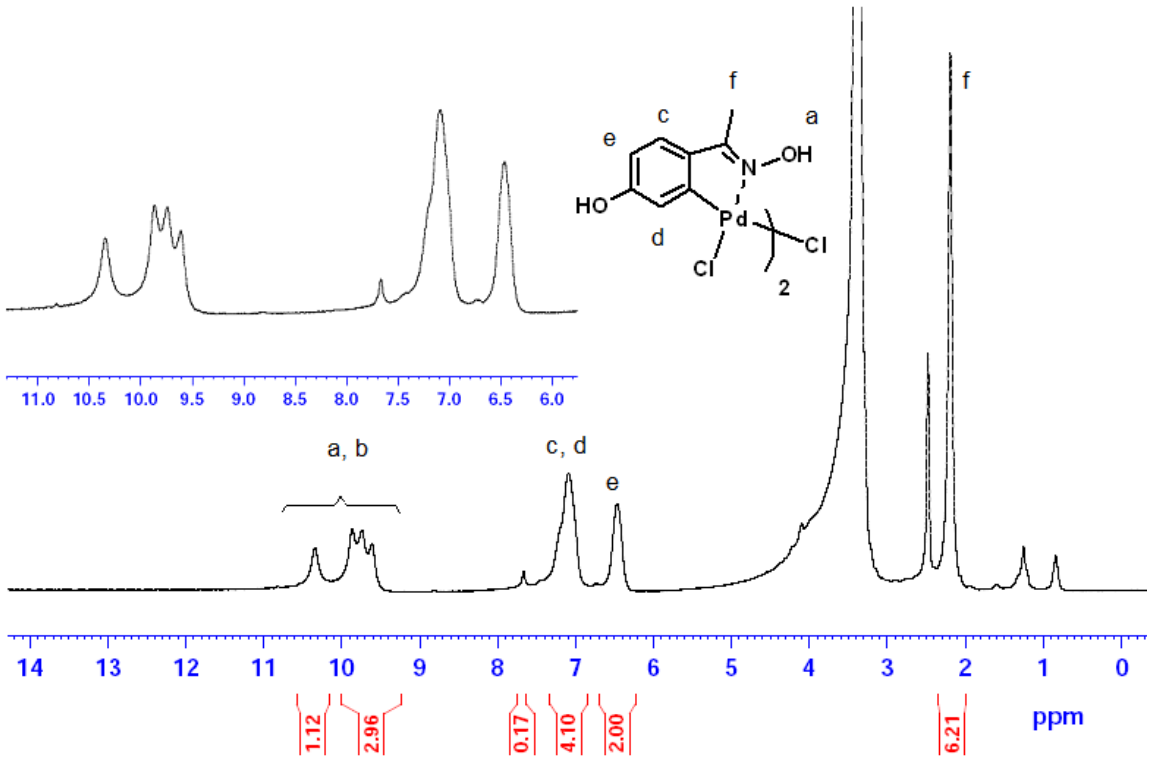

Figure S4. ^{1}H NMR spectrum (250 MHz, DMSO-d_6) of 4-hydroxyacetophenone oxime-derived palladacycle

D. NMR Spectra of the Mizoroki-Heck cross-coupling reaction products.

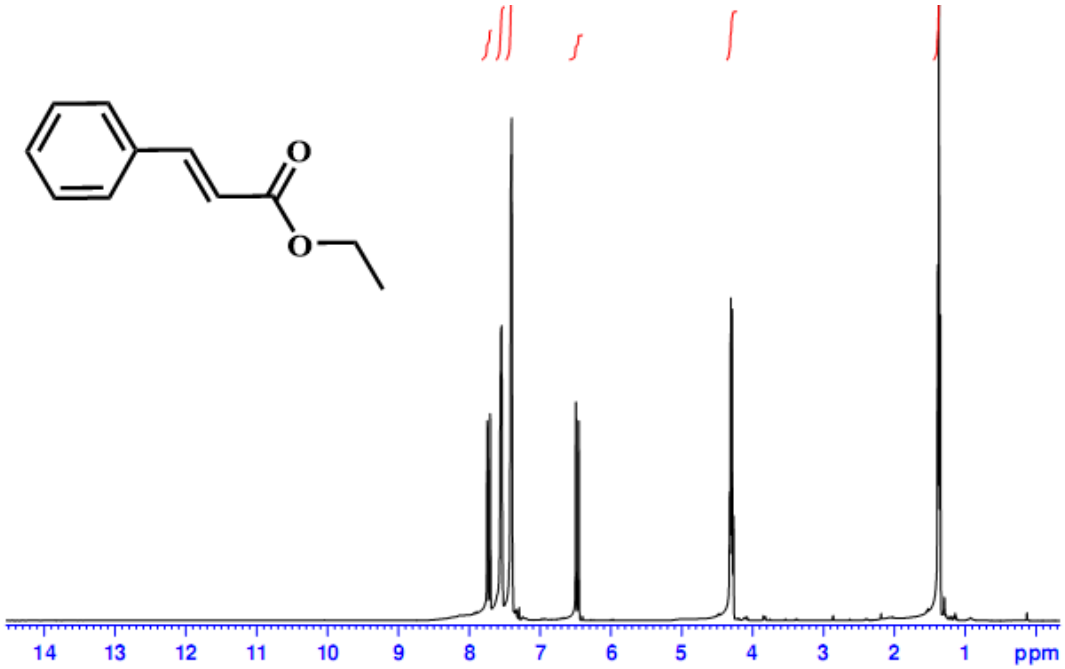

Figure S5. ^{1}H NMR spectrum of ethyl cinnamate 3a (400 MHz, $CDCl_3$).

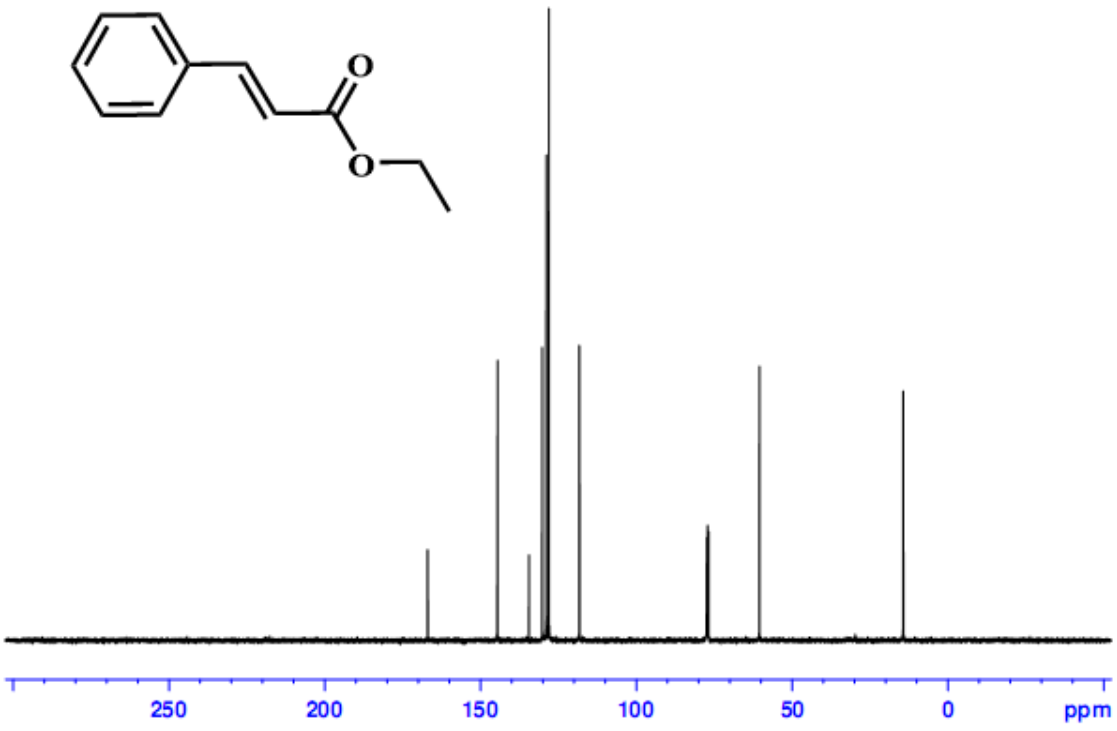

Figure S6. ^{13}C NMR spectrum of ethyl cinnamate 3a (100 MHz, $CDCl_3$).

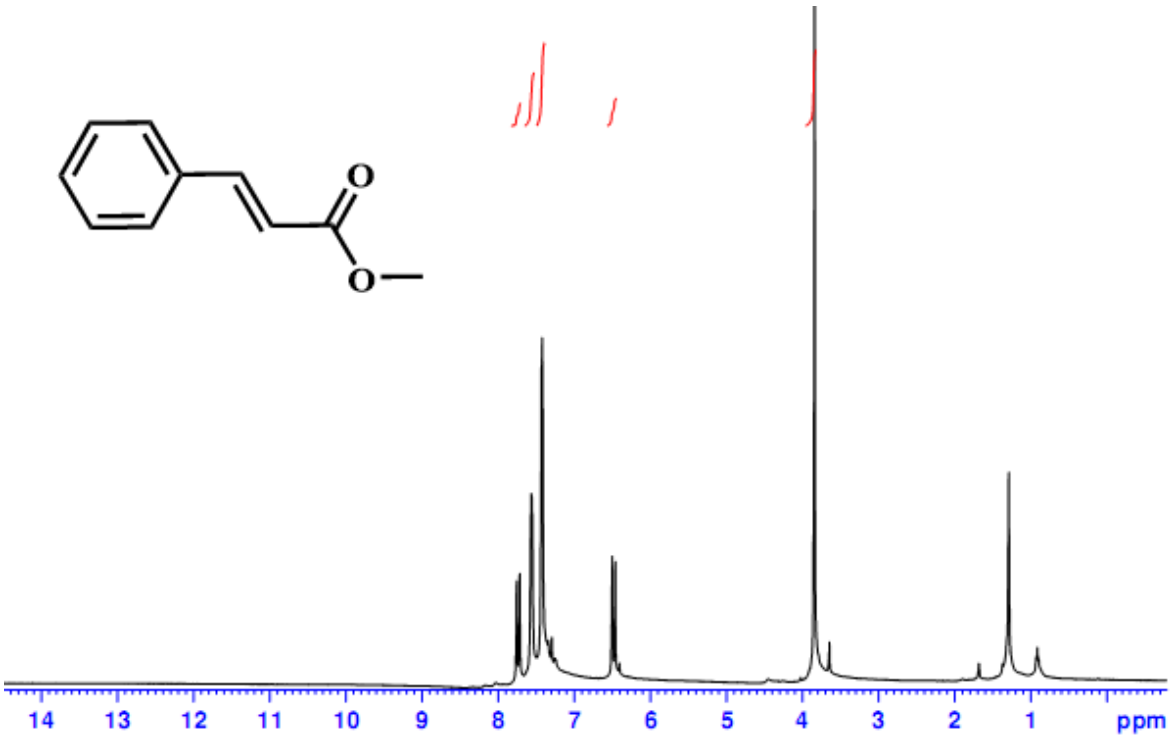

Figure S7. ^{1}H NMR spectrum of methyl cinnamate 3b (400 MHz, $CDCl_3$).

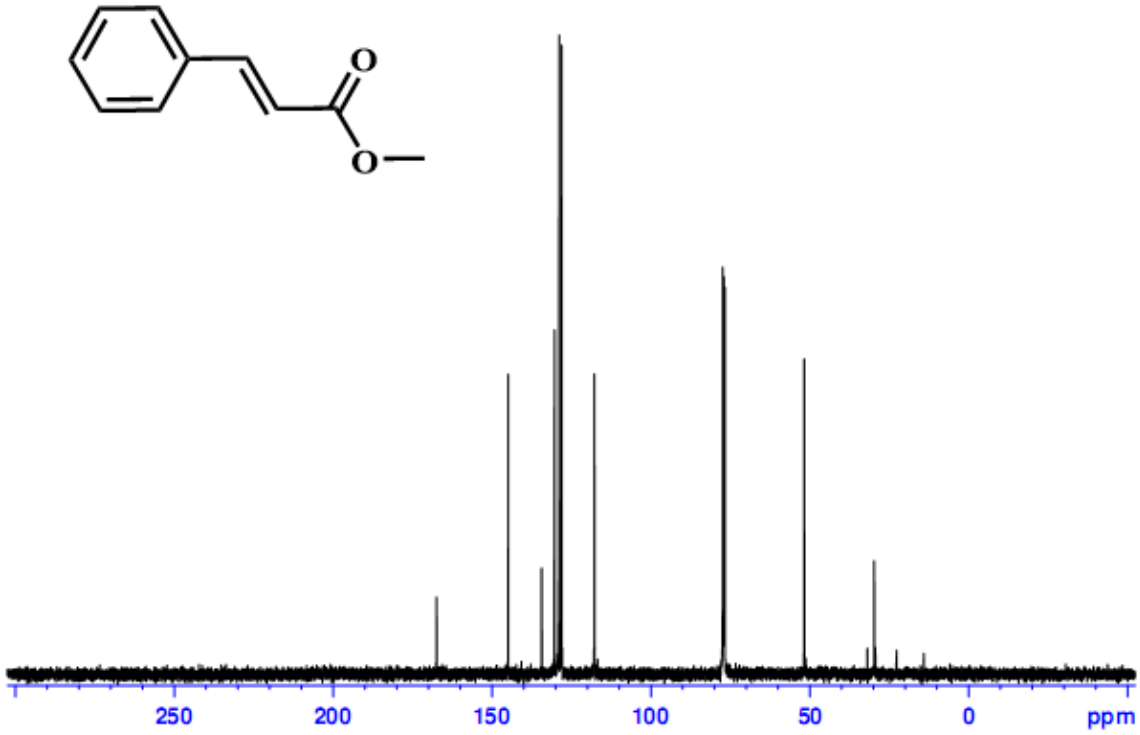

Figure S8. ^{13}C NMR spectrum of methyl cinnamate 3b (100 MHz, $CDCl_3$).

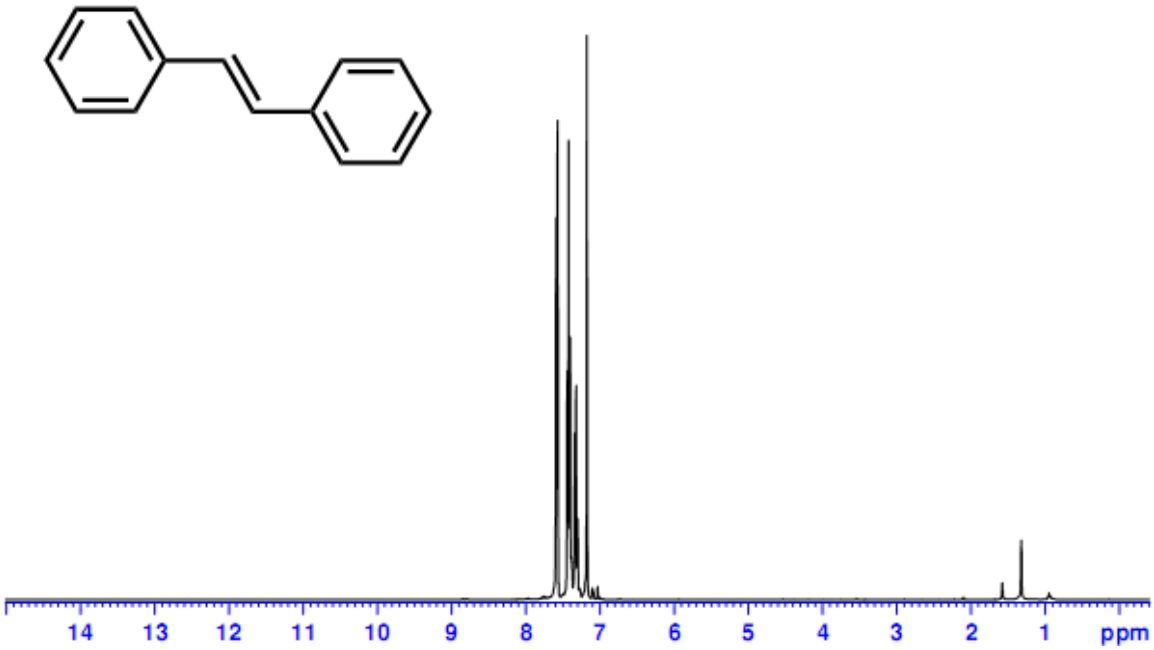

Figure S9. ^{1}H NMR spectrum of (E)-1,2-diphenylethene 3c (400 MHz, $CDCl_3$).

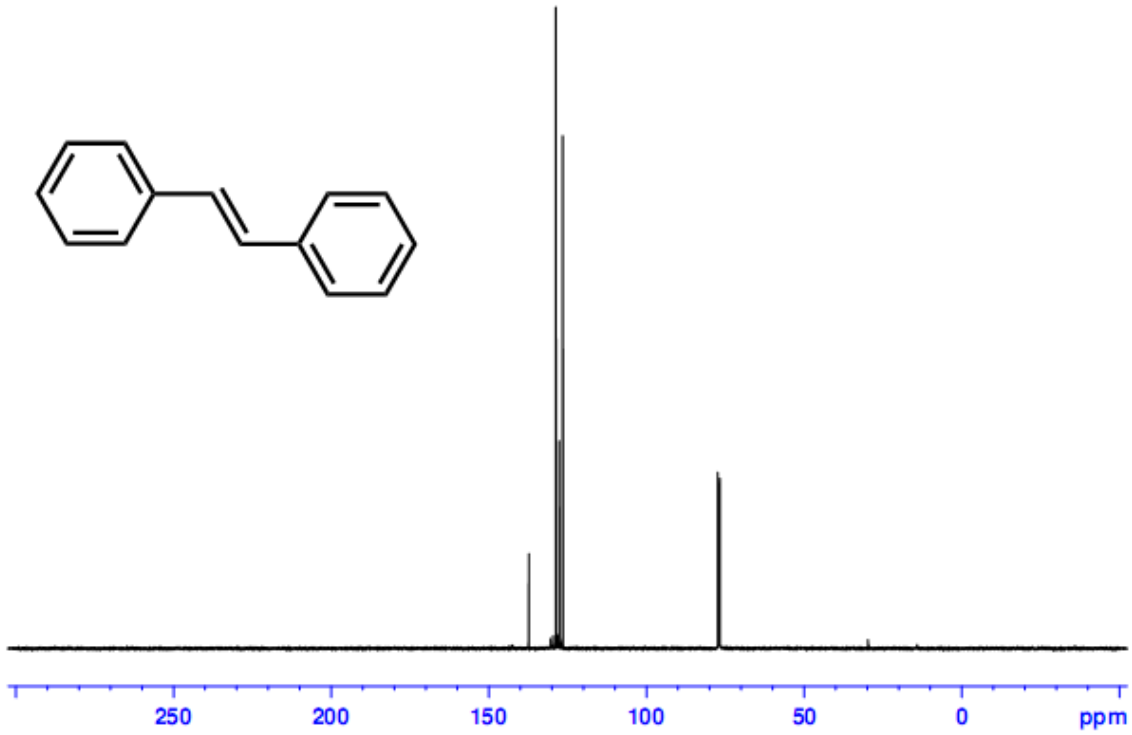

Figure S10. ^{13}C NMR spectrum of (E)-1,2-diphenylethene 3c (100 MHz, $CDCl_3$).

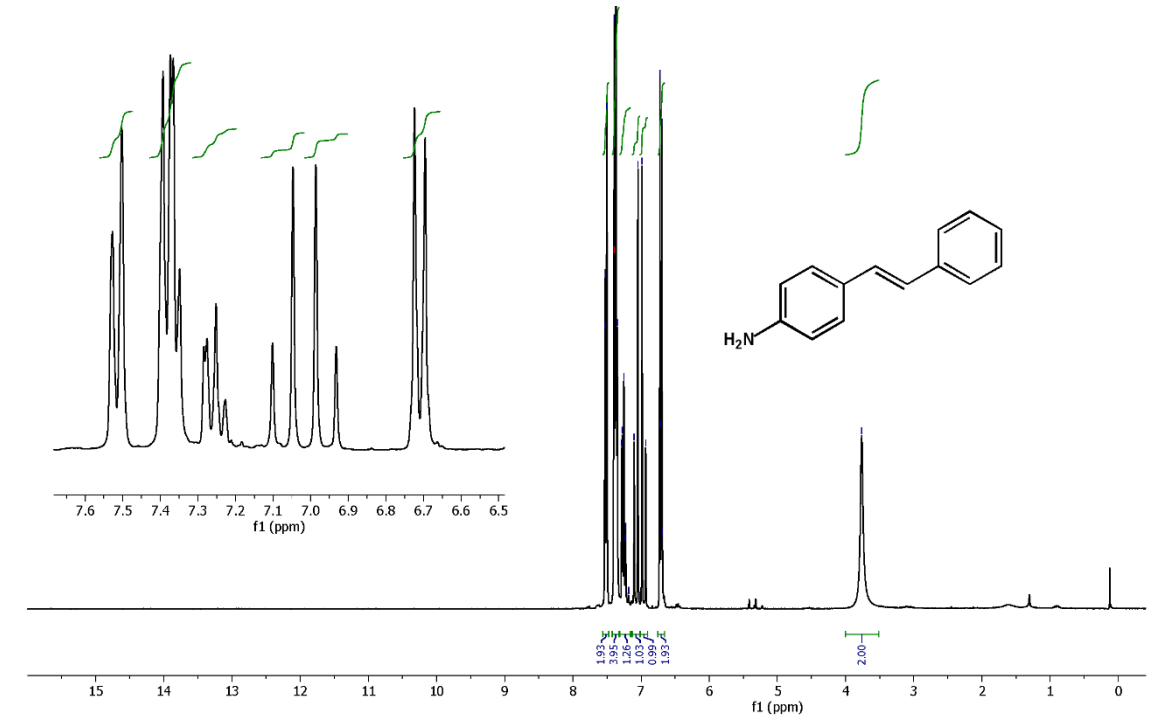

Figure S11. ^{1}H NMR spectrum of (E)-4-styrylaniline 3f (300 MHz, $CDCl_3$).

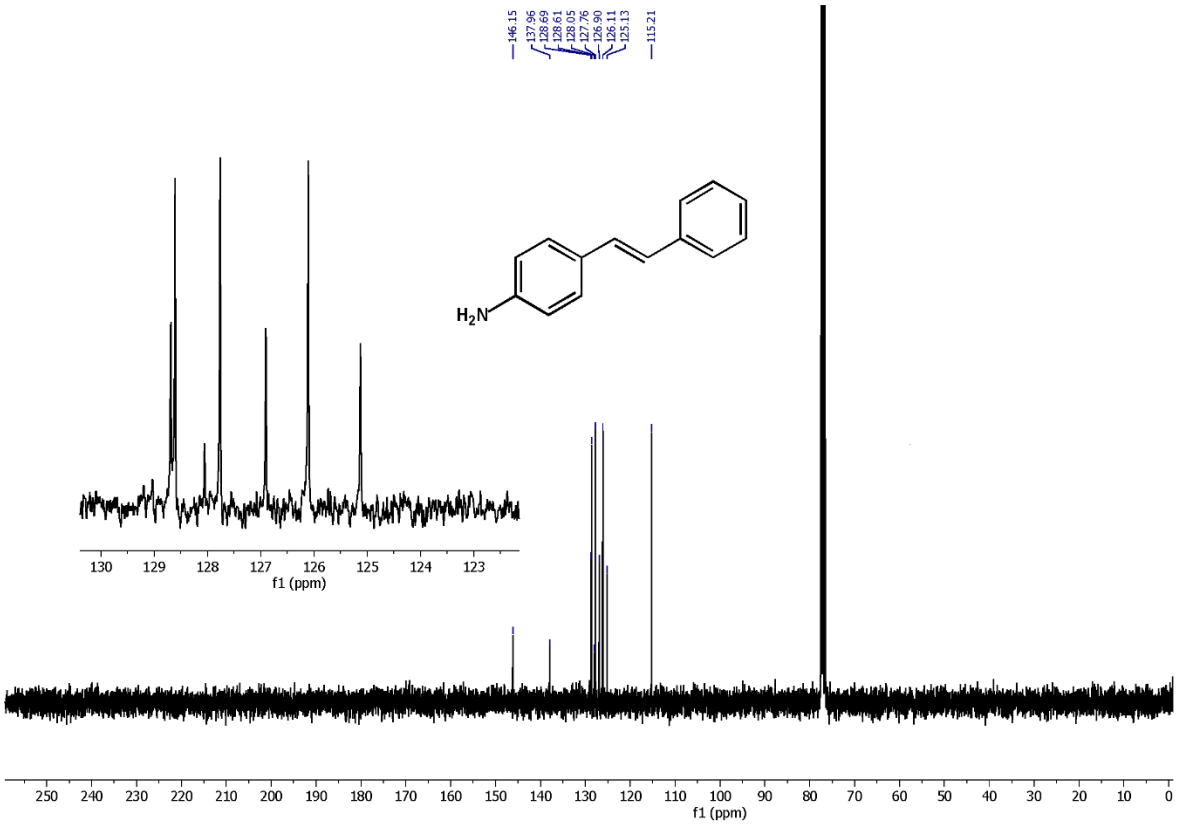

Figure S12. ^{13}C NMR spectrum of (E)-4-styrylaniline 3f (62.5 MHz, $CDCl_3$).

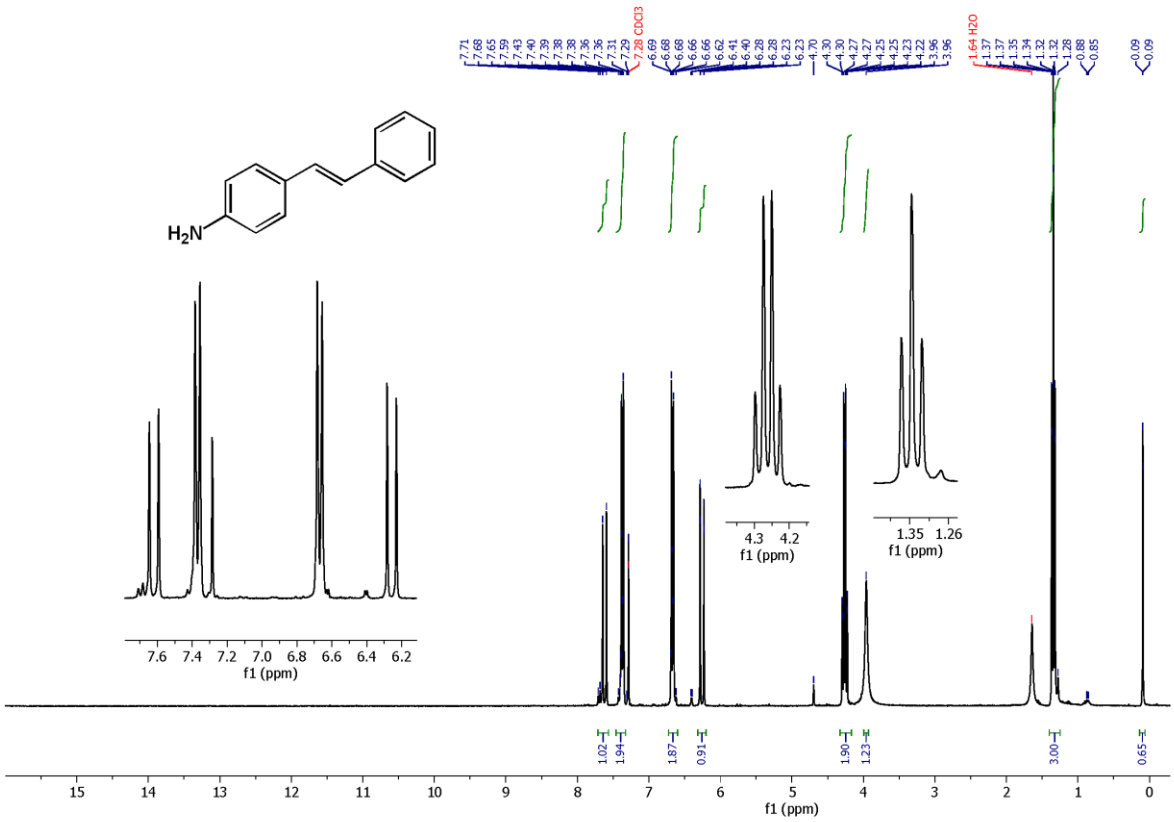

Figure S13. ^{1}H NMR spectrum of ethyl (E)-3-(4-aminophenyl)acrylate 3g (300 MHz, $CDCl_3$).

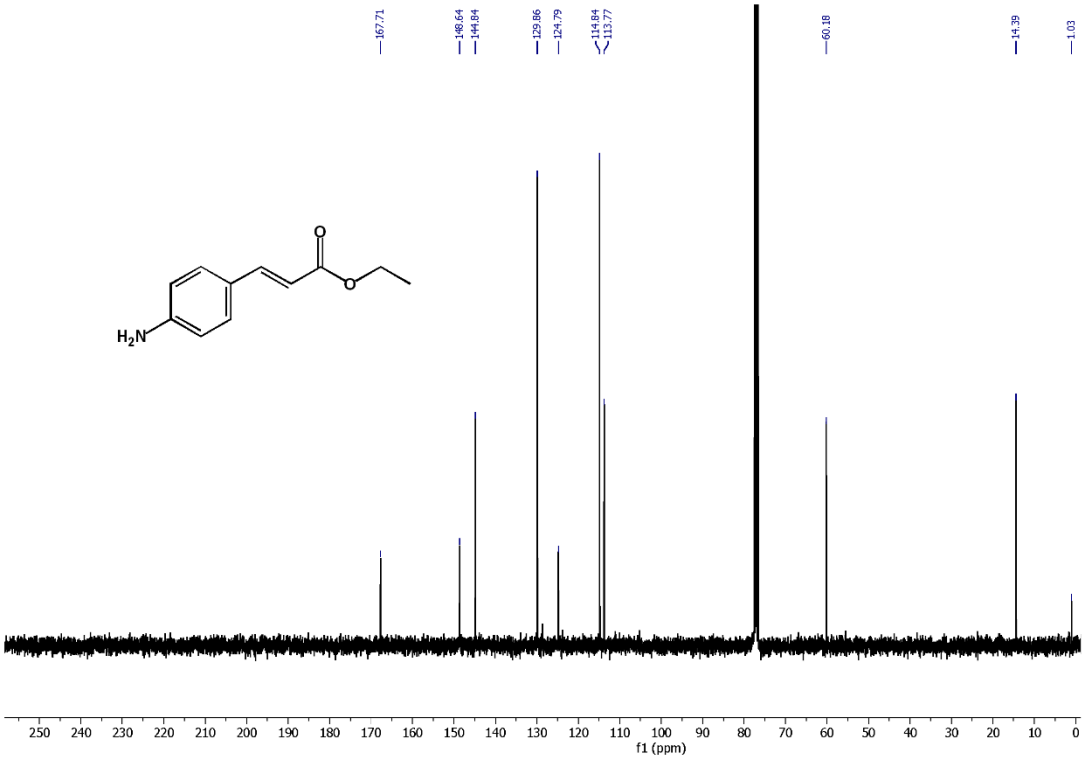

Figure S14. ^{13}C NMR spectrum of ethyl (E)-3-(4-aminophenyl)acrylate 3g (62.5 MHz, $CDCl_3$).

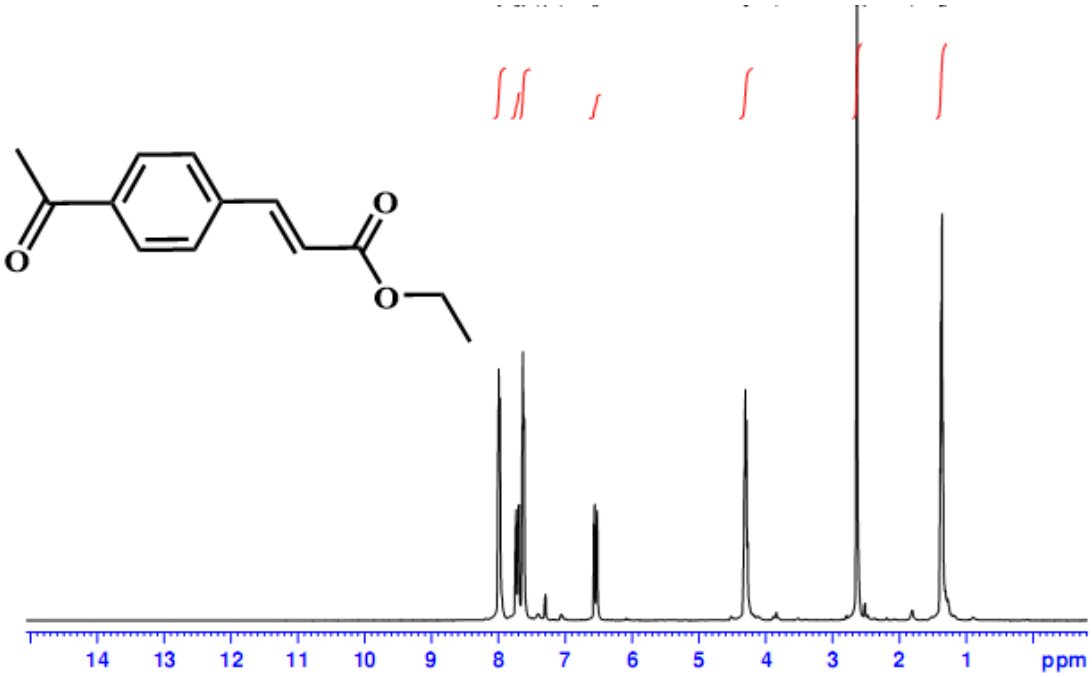

Figure S15. ^{1}H NMR spectrum of ethyl (E)-3-(4-acetylphenyl)acrylate 3h (400 MHz, $CDCl_3$).

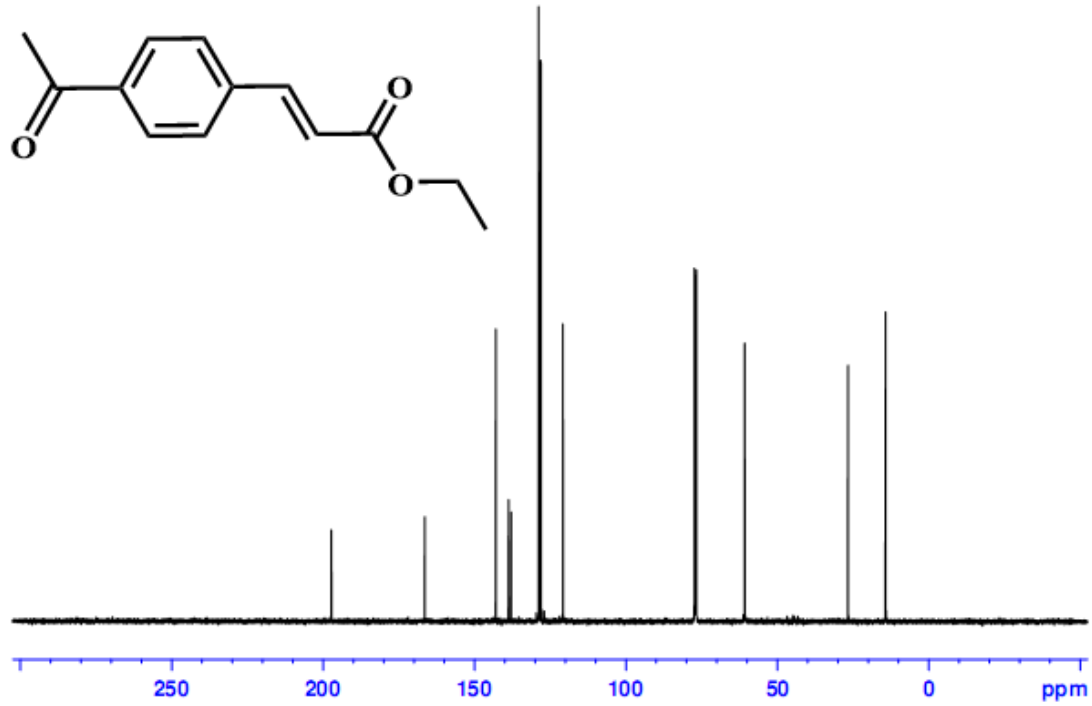

Figure S16. ^{13}C NMR spectrum of ethyl (E)-3-(4-acetylphenyl)acrylate 3h (100 MHz, $CDCl_3$).

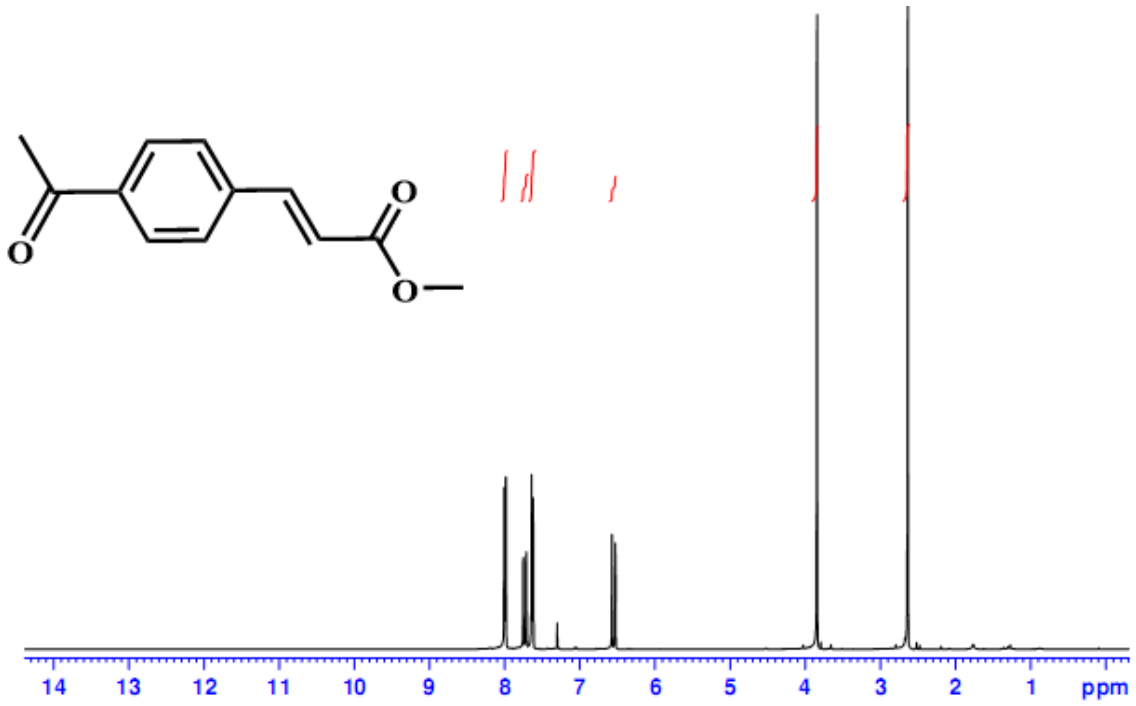

Figure S17. ^{1}H NMR spectrum of methyl (E)-3-(4-acetylphenyl)acrylate 3i (400 MHz, $CDCl_3$).

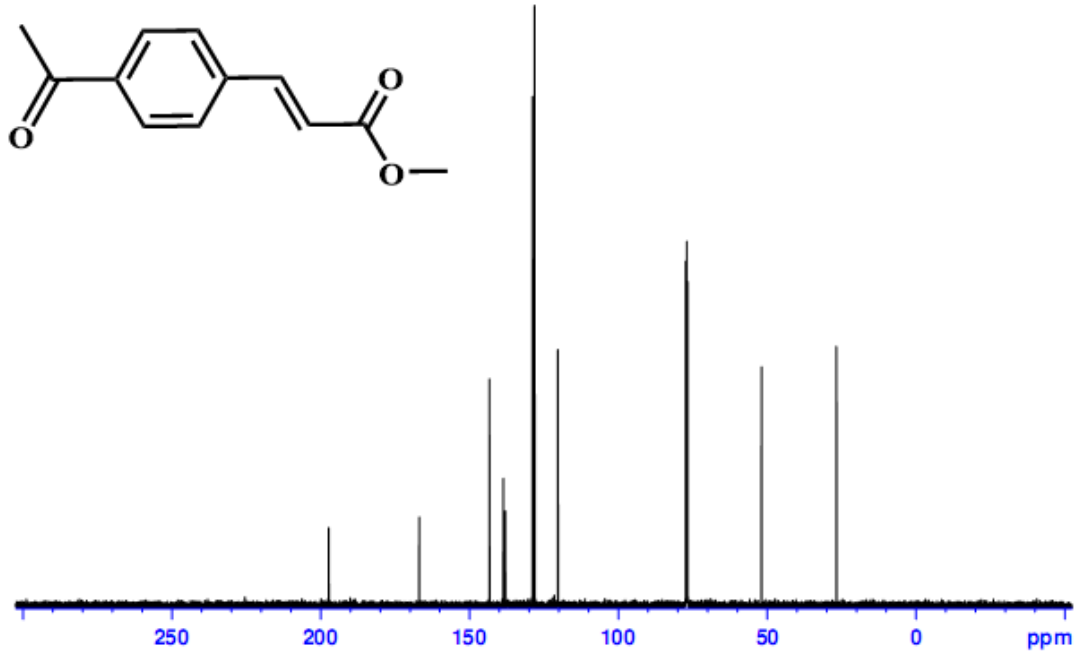

Figure S18. ^{13}C NMR spectrum of methyl (E)-3-(4-acetylphenyl)acrylate 3i (100 MHz, $CDCl_3$).

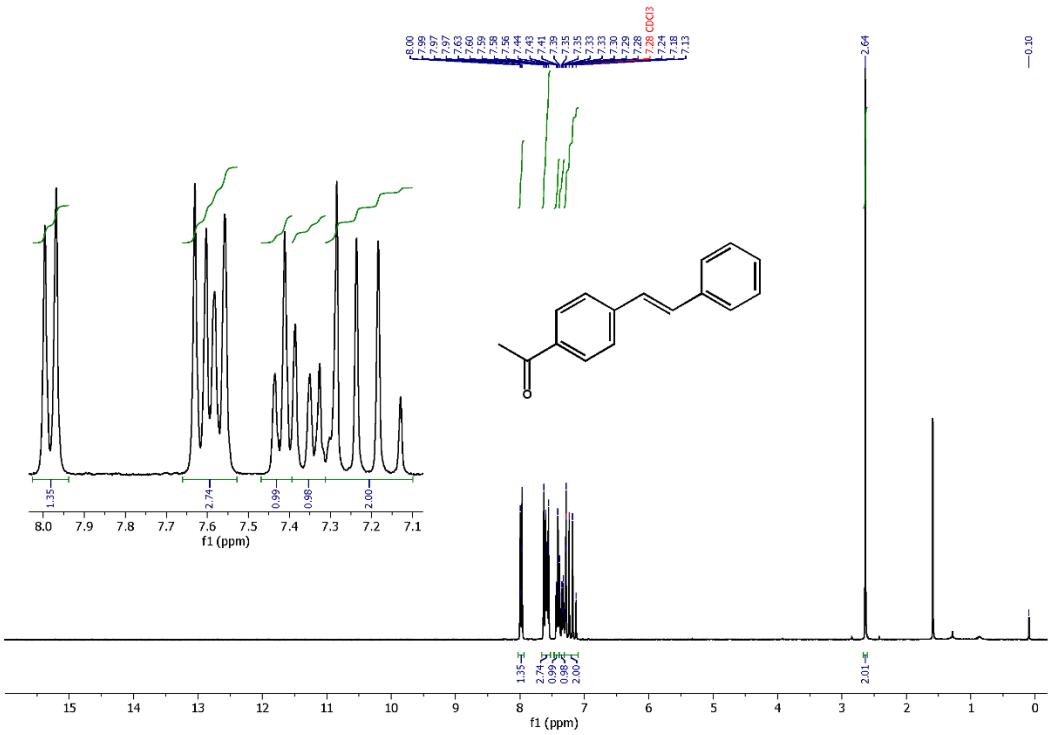

Figure S19. ^{1}H NMR spectrum of ethyl (E)-1-(4-styrylphenyl)ethan-1-one 3j (300 MHz, $CDCl_3$).

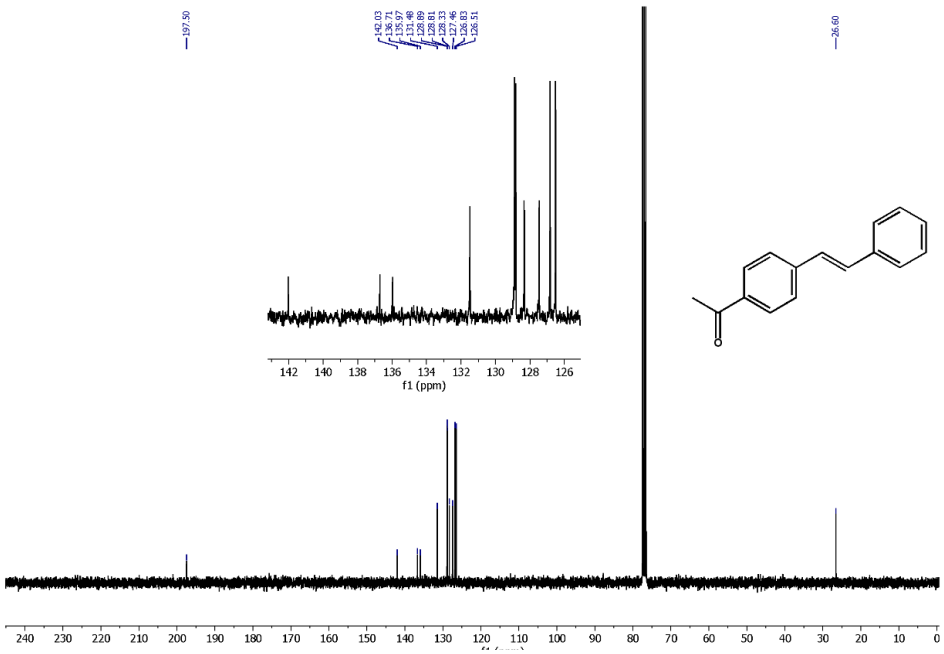

Figure S20. ^{13}C NMR spectrum of ethyl (E)-1-(4-styrylphenyl)ethan-1-one 3j (62.5 MHz, $CDCl_3$).

References

[1] Y. Mansoori, A. Khodayari, A. Banaei, M. Mirzaeinejad, Y. Azizian-Kalandaragh and M. Pooresmaeil, RSC Adv., 6 (2016) 48676.

[2] S. Wang, K. Wang, C. Dai, H. Shi and J. Li, Chem. Eng. J., 262 (2015) 897.

[3] A. Nuri, Y. Mansoori and A. Bezaatpour, Appl. Organomet. Chem., 33 (2019) e4904.

[4] P.K. Byers, A.J. Canty, H. Jin, D. Kruis, B.A. Markies, J. Boersma and G. Van koten, Organometallics, 14 (1995) 4213.

[5] W.L.F. Armarego and C.L.L. Chai, *Purification of laboratory chemicals (*Butterworth-Heinemann, Burlington, 2003)

[6] M. Sajedi, Y. Mansoori, A. Nuri, S. Fekri, D. Esquivel and M.A. Navarro, Catal. Surv. Asia, (2022).

[7] D. Zhao, J. Feng, Q. Huo, N. Melosh, G.H. Fredrickson, B.F. Chmelka and G.D. Stucky, Science, 279 (1998) 548.

[8] J. Mondal, S. Sreejith, P. Borah and Y. Zhao, ACS Sustain. Chem. Eng., 2 (2014) 934.

[9] M. Khabazipour, S. Shariati and F. Safa, Synth. React. Inorg. M., 46 (2016) 759.